DOI 10.1515/htmp-2013-0082 — High Temp. Mater. Proc. 2014; 33(6): 571–584

Miia Kiviö*, Lauri Holappa, Takeshi Yoshikawa and Toshihiro Tanaka

Interfacial Phenomena in Fe/Stainless Steel–TiC Systems and the Effect of Mo

Abstract: Titanium carbide is used as reinforcement particles in composites due to its hardness, wear resistance and stability. This work is a part of the study in which titanium carbides are formed in stainless steel castings in the mold to improve the wear resistance of a certain surface of the casting. Such local reinforcement is a very potential method but it is a quite demanding task requiring profound knowledge of interfacial phenomena in the system, wettability, stability, dissolution and precipitation of new phases in production of these materials. Good wetting between different constituents in the material is a key factor to attain maximal positive effects. Mo is used with TiC or Ti(C,N) reinforcement in composites to improve wettability. In this work the effect of Mo on the phenomena in Fe/stainless steel–TiC systems was examined by wetting experiments between the substrate and the alloy. Wetting was not significantly improved by adding Mo to the systems. Core-rim type carbides as well as more homogenous carbide particles were observed. Overall the carbide particles are very complex regarding to their chemistry, size and shape which aspects have to be taken into account in the development of these materials and manufacturing processes.

Keywords: titanium carbide, molybdenum, stainless steel, reinforcement, interfacial phenomena, wetting

PACS® (2010). 68.08.Bc

***Corresponding author: Miia Kiviö:** Research Group of Metallurgy, Department of Materials Science and Engineering, School of Chemical Technology, Aalto University, Aalto 00076, Finland. E-mail: miia.kivio@aalto.fi

Lauri Holappa: Research Group of Metallurgy, Department of Materials Science and Engineering, School of Chemical Technology, Aalto University, Aalto 00076, Finland

Takeshi Yoshikawa: Department of Materials and Environmental Science, Institute of Industrial Science, University of Tokyo, Tokyo 153-8505, Japan

Toshihiro Tanaka: Division of Materials and Manufacturing Science, Graduate School of Engineering, Osaka University, Osaka 565-0871, Japan

1 Introduction

TiC is a well-known reinforcement material used in metal-matrix composites. TiC is considered a good reinforcement material due to its hardness and stability. It is also known for resistant to high temperature oxidation and stability in corrosive environments. TiC can be used e.g. in stainless castings to improve the hardness and wear resistant of the material. If the reinforcement material is added only locally on the surface, which acquires wear resistance, the whole material does not need to be reinforced. This process results in a stainless casting with hard surface combined with a tough matrix. In this method [1] a titanium and carbon mixture is placed before casting of the steel in the mold on the surface which acquires wear resistance. During casting the heat of the molten metal sets off the reaction between Ti and C to form TiC by self-propagating high temperature synthesis (SHS). Wettability, stability and dissolution of the reinforcement particles play key roles in adding them to liquid steel as well as developing the process and the materials. Especially wetting is important in producing these metal-matrix composites. A low contact angle denotes good wettability ensuring good bonding between the reinforcement particles and matrix metal and a desired distribution of the reinforcement particles in the melt.

Chromium, nickel and molybdenum are typical alloying elements in stainless steels. The effect of Cr and Ni on the interfacial phenomena in Fe-TiC systems has been discussed in the previous article by the authors [2]. In this study the effect of Mo on the interfacial phenomena in Fe-TiC systems is examined. It is well known that addition of alloying elements like Ti and Mo to stainless steel results in formation of titanium and molybdenum carbides and reduced formation of chromium containing carbides [3–4]. According to Pardo et al. [4] the presence of molybdenum in the stainless steel reduces precipitations of chromium rich carbides. Mo stabilizes TiC in the steel and replaces Cr in the carbides leading to reduced Cr depletion in the stainless steel which further leads to improved corrosion resistance. On the other hand, formation of Mo precipitates results in Mo depletion in the material and decreases the passive properties of the stainless steel. The increased carbon content and the formation of CrC_x

were discussed in detail in the previous article by the authors [2]. Jang et al. [5] have also reported that carbon is partly replaced by vacancies in the (Ti,Mo)C resulting in an increased solute carbon concentration.

Mo is believed to improve wettability and is commonly added to reinforcement [6–10]. Mo_2C has the lowest negative heat of formation among carbides resulting in the lowest contact angles with liquid metals [8]. Several studies about the addition of Mo to composites and cermets with TiC have been done [7, 9–16]. The core-rim structure in Ti(C,N) cermets containing molybdenum is well-known [6, 8–10, 13]. It consists of a Ti(C,N) core with a (Ti,Mo)(C,N) type carbonitride rim surrounding the core. Molybdenum is added as Mo_2C to TiC based materials to improve wettability especially in Ni based cermets [7, 13, 16]. Usually 10–25 mass% of Mo_2C is added into Ti(C,N) [16]. The Mo_2C reacts during sintering to form mixed (Ti,Mo) carbides and/or carbonitrides which exist as rims around the TiC and Ti(C,N) particles. It also partly dissolves into the binder material [16]. Addition of Mo has been reported to decrease the grain size of the carbides [6, 8] and resulting in a more homogenous structure of NiMo-TiC based alloys [6]. Cutard et al. [13] reported that addition of Mo into TiC and Ti(C,N) cermets decreases the grain size of the TiC and Ti(C,N) by decreasing dissolution of the Ti(C,N) and by decreasing growth rate of the (Ti,Mo)C rim surrounding the particles. Hussainova [14] added Mo with the binder material Ni and observed improved interface bond strength and improved wear resistance due to Mo addition. The decreasing of coarsening of TiC and Ti(C,N) due to Mo addition has also been observed by other studies [14–15].

(Ti,Mo)C particles in steel improve hardness compared to TiC and they have an excellent thermal stability [17]. Erauskin et al. [18] have studied addition of Fe(TiMo)C master alloys to liquid austenitic Mn steel in liquid state before casting followed by heat treatment and quenching. The (TiMo)C particles remained almost unchanged after addition to the melt, casting and heat treatment indicating high stability. Addition of molybdenum to Ti bearing low-alloyed steels in order to produce nano-sized (Ti,Mo)C carbides has also been studied by several authors [5, 17, 19]. Yield strengths up to 600 MPa have been achieved in HSLA steel with nano-sized Ti and Mo containing carbides which is significantly higher than in conventional Ti bearing steels. The effective size of the carbides was 5–10 nm. The carbides contained similar at% of Ti and Mo and Funakawa et al. [19] concluded that the best mechanical properties were obtained with a Ti/Mo atomic ratio of 1 in the steel. Addition of Mo to the steel resulted in decreased size of the carbides [5, 17]. Evtushenko et al. [20] studied fabrication of tool steel with TiC and Mo addition by SHS method and concluded that a fine initial grain size of the TiC results in a dense and less porous ingot.

In this paper the effect of Mo on the interfacial phenomena in Fe-TiC systems as well as the interfacial phenomena between stainless steel 304 and TiC or TiCMo have been studied. TiCMo is a TiC substrate alloyed with Mo. Wetting, stability, dissolution and other phases and structures formed in the systems have been discussed. The results of this study concerning interfacial phenomena in these systems are essential information in developing the TiC or TiCMo reinforced materials and their production methods. This work is part of a study related to producing stainless steel castings which have been locally reinforced with TiC or TiCMo by SHS method [1].

2 Experimental procedures

Wetting experiments in Fe-TiC-Mo systems and in TiC/TiCMo-stainless steel systems have been performed in order to get information on the wettability, stability, dissolution and resulting microstructure of the systems. The substrates (TiC and TiCMo) were prepared from powders by spark plasma synthesis (SPS) to form dense substrates [2]. The TiCMo substrates were prepared from SHS-TiC powder alloyed with Mo. The Mo content of the powder was 14 mass%. The metal and metal alloys used as the liquid material were prepared by melting iron and the alloy metal powders together to form an alloy which was cut to suitable pieces after solidification [2]. Two types of wetting experiments were performed: type A and type B. In type A experiments the substrate and the metal or metal alloy were placed inside a furnace and heated up to approximately 1823 K in Ar-1%H_2 atmosphere at 4.17 K/min. The measurement of the contact angle started when the metal/alloy droplet was completely molten. This point was considered t = 0 and it was the initial contact angle. The sample was kept at 1823 K for 15–30 min and after the holding period cooled down to room temperature at 4.17 K/min. The contact angle was measured during the whole holding period until the droplet was solidified during cooling. In type B experiments the substrate was heated inside the furnace to 1823 K in Ar-10%H_2 atmosphere at an average of 10.2 K/min. The metal/alloy to be used as the droplet was kept outside the furnace and not heated together with the substrate. When the furnace had reached the experimental temperature 1823 K the metal/alloy was moved inside the furnace and let to melt down above the substrate in a separate tube and once it was molten the droplet fell on the top of the substrate. The

contact angle was measured immediately after the droplet fell on the substrate and this was considered t = 0 and the initial contact angle. The sample was kept at 1823 K for 3–10 min and after that cooled down to 1673 K fast and then from 1673 to room temperature at approximately 9.8 K/min. The contact angle was measured during the whole holding period until the droplet was solidified during cooling. The experimental procedures were explained in detail in a previous article by the authors [2]. The main difference between type A and type B experiments was that in type A the substrate and the alloy droplet were heated together in contact with each other to the holding temperature and in type B experiments they were heated separately and the molten alloy droplet was dropped on the top of the substrate when the temperature had reached the holding temperature. Hence in type B experiments no reactions between the substrate and the alloy droplet took place during the heating. The holding period in type A experiments was slightly longer than in type B and the cooling rate of the samples in type B experiments was higher than in type A. Type B experiments resembled more the actual casting process of the composites [1]. After the experiments the samples were cut, ground and polished to study the cross-section with a scanning electron microscope and energy dispersive spectroscopy (SEM-EDS) with LEO SEM 1450, EDS analyser from Oxford Instruments and INCA Software version 17B by using 15 kV as an accelerating voltage.

A summary of the experiments is presented in Table 1.

Experiments with pure Fe and a TiCMo substrate were performed with two different holding periods (3 and 10 min) to study the dissolution and infiltration similarly as in Fe-TiC systems in the previous study by the authors [2]. Also three experiments with stainless steel as the droplet material have been performed. Stainless steel was chosen because it is a potential material for the applications of TiC reinforcement [1]. The stainless steel was 304, which is a common stainless steel grade. The analysis is represented in Table 2. Due to the bigger particle size of the powder used as raw material for the substrates, the density is somewhat lower in the TiCMo substrates and the substrate used in experiment 9. This is noteworthy although according to Samsonov et al. [21] the porosity up to 8% should not affect wetting. Experiments 1 and 5 were presented and discussed in the previous article by the authors [2]. They are presented here as reference experiments.

Table 2: Analysis of the 304 stainless steel used in the experiments (in mass%)

C	Mn	Si	Cr	Ni	Mo	Al	N	S
0.008	0.93	0.51	19.9	9.3	0.29	<0.017	0.0181	0.03

The wetting experiments were partly performed at Aalto University School of Chemical Technology (type A) [22] and partly at Osaka University (type B). All the analyses were done at Aalto University.

3 Results and discussion

3.1 Contact angles

Figures 1–3 represent the contact angles in type A experiments, type B experiments and in experiments with stainless steel respectively. In type A experiments (Fig. 1) alloying Fe with Mo clearly resulted in lower contact angles. The initial contact angles (at t = 0) were higher with Fe-Mo but they dropped to around 20° very quickly. The increase in the Mo content of the Fe-alloy from 3.7 mass% to 5.2 mass% did not have an effect on the wettability. In experiment 1 (Fe-TiC A) slight carbide formation and solidification of the droplet was observed towards the end of the experiment starting after 12 min holding [2]. In experiments 2 and 3 (FeMo5.2-TiC A and FeMo3.7-TiC A) no

Table 1: Summary of the experiments

Experiment number	Experiment type	Experiment abbreviation	Metal droplet alloy mass%	Substrate type	Substrate density (%)	Holding period (min)	Holding temperature (K)
1	A	Fe-TiC A	Fe	TiC	98	30	1823
2	A	FeMo5.2-TiC A	FeMo5.2	TiC	98	15	1823
3	A	FeMo3.7-TiC A	FeMo3.7	TiC	98	15	1823
4	A	304-TiC A	304	TiC	98	15	1748
5	B	Fe-TiC B	Fe	TiC	98	10	1823
6	B	Fe-TiCMo B	Fe	TiCMo	92	10	1823
7	B	Fe-TiCMo B 3	Fe	TiCMo	92	3	1823
8	B	FeMo3.5-TiC B	FeMo3.5	TiC	98	10	1823
9	B	304-TiC B	304	TiC	92	10	1823
10	B	304-TiCMo B	304	TiCMo	92	10	1823

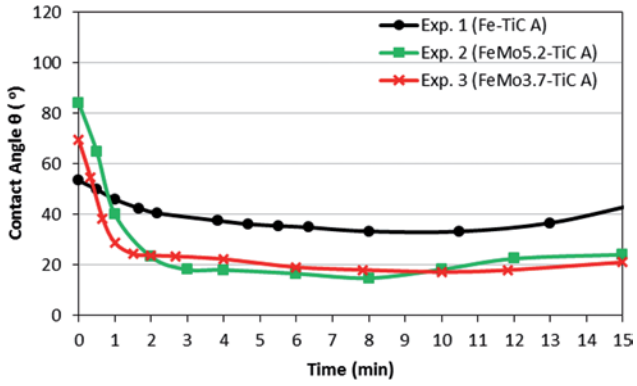

Fig. 1: Contact angles vs. time in type A experiments

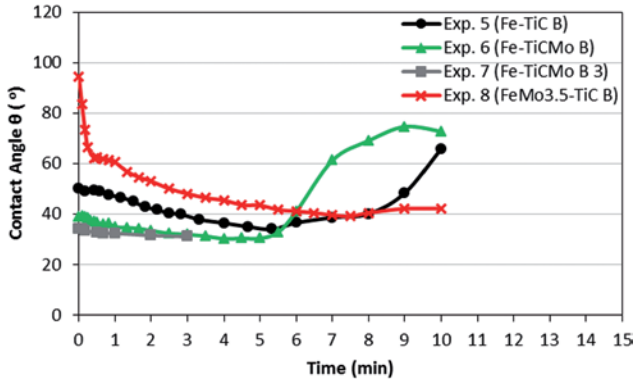

Fig. 2: Contact angles vs. time in type B experiments

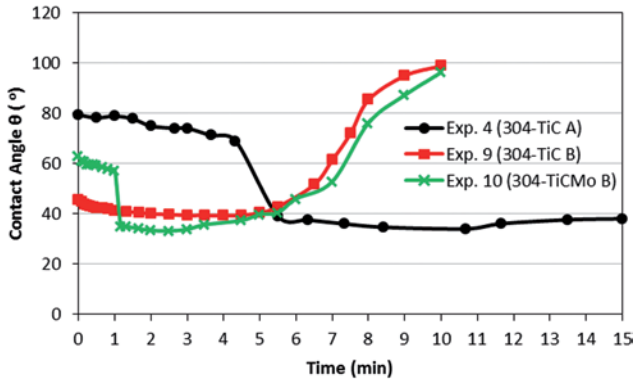

Fig. 3: Contact angles in experiments with stainless steel

carbide formation during the holding period was observed. The formation of TiC from Fe-Ti melt and solid graphite followed by floatation of the TiC particles has been reported also in other studies [23].

In type B experiments (Fig. 2) alloying Fe with Mo did not improve wetting. The initial contact angle (at t = 0) in experiment 8 (FeMo3.5-TiC B) was clearly higher. The initial contact angle dropped quickly and the minimum contact angle was slightly higher than in experiment 5 (Fe-TiC B). The contact angle in experiment 8 was clearly higher than in type A experiments 2 and 3 with similar alloys. The reason is most likely the reactions during heating in type A experiments. Using TiCMo substrate in experiments 6 (Fe-TiCMo B) and 7 (Fe-TiCMo B 3) instead of TiC did not have a strong effect on the wetting either. The increase of the contact angle at around 5–6 min in experiment 6 is due to carbide formation and solidification of the surface of the droplet. In experiment 7 there was no time for carbide formation to take place during the short (3 min) holding period and only during cooling slight carbide formation was observed on the droplet.

Overall the experiments with Fe-Mo alloys (experiments 2, 3 and 8) did not show strong carbide formation during the holding period. But during solidification stronger carbide formation was observed (Fig. 4 and 5). In Fig. 4 almost no solidification due to carbide formation can be observed on the surface of the liquid droplet during the

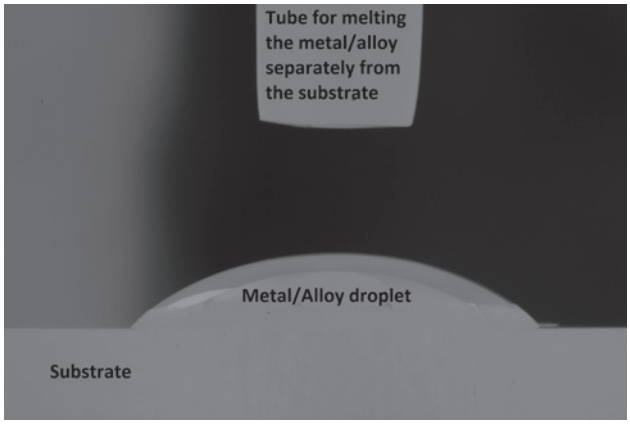

Fig. 4: The droplet form in experiment 8 (FeMo3.5-TiC B) after 10 min holding at 1823 K

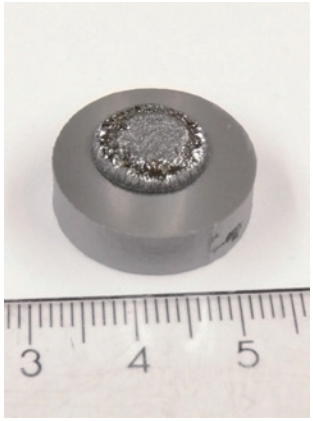

Fig. 5: The droplet and the substrate of experiment 8 (FeMo3.5-TiC B) after the experiment

holding period. But from Fig. 5 it is clearly observed that the surface of the solidified droplet is not smooth indicating carbide formation during solidification. The samples were cooled down to 1673 K at 50 K/min and from that to room temperature more slowly 9.8 K/min [2].

The minimum contact angles in the experiments with stainless steel are similar even though the temperature in experiment 4 (304-TiC A) was clearly lower (Table 1). The combined effect of the reactions during heating and the lower temperature result in similar minimum contact angles between all the experiments. Neither do they differ from the contact angles of pure Fe experiments with TiC or TiCMo substrates. In experiments 9 and 10 (304-TiC B and 304-TiCMo B) the contact angle is strongly increased as a result of TiC formation on the droplet and solidification of the droplet surface. In experiment 4 no carbide formation during the holding period was observed but during solidification the formation of carbides on the surface of the droplet was strong. The reason is probably the lower holding temperature due to which there is no time for the TiC to form and drift to the surface.

3.2 Penetration zone

The penetration depth of the melt (Fig. 6) into the substrate was quite strong in all experiments except for experiment 7 (Fe-TiCMo B 3) due to the short holding time. Also the high roughness of the interface observed in all experiments suggests strong dissolution of the substrate into the melt and a strong infiltration of the melt into the substrate. In A type experiments (1–4) the reactions during heating have resulted in stronger penetration of the melt and dissolution of the substrate. Experiment 4 (304-TiC A) has the strongest penetration due to the existence of Cr and Ni in the steel. It is clearly stronger than the penetration of 304 in type B experiments 9 and 10 as a consequence of the reactions during heating, longer holding period and smaller cooling rate in the type A experiments. Alloying Fe with Mo clearly improves penetration compared to pure Fe. Adding Mo into the TiC substrate does not have such a clear effect. Penetration of Fe into TiC is better than into TiCMo. The penetration of stainless steel into TiCMo is slightly better than into TiC. Probably the presence of Ni in steel leads to similar outcome between TiCMo or TiC with stainless steel. In the previous article by the authors [2] it was presented that the alloys containing Ni had the strongest penetration of the melt and the dissolution of the substrate and even the FeCr alloys had higher penetration depths than the FeMo alloys. Figure 7 represents the substrate before the experiment and Figures 8 and 9 represent the penetration zones of TiCMo in experiment 6 (Fe-TiCMo B) and TiC in Experiment 8 (FeMo3.5-TiC B), respectively. The substrate before the experiment is

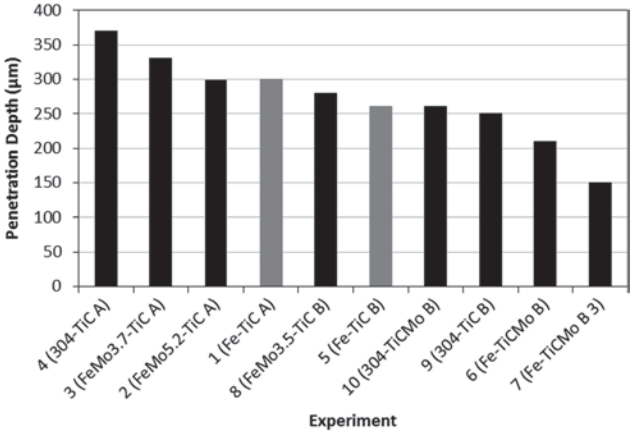

Fig. 6: Penetration depths of the melt into the substrate

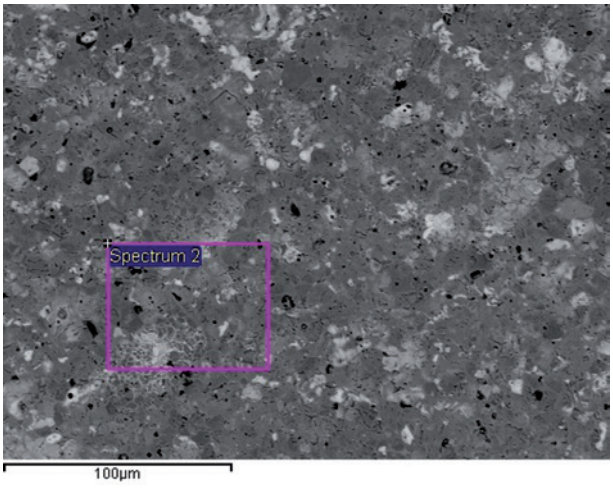

Fig. 7: SEM-BSE image of the TiCMo substrate before the experiment

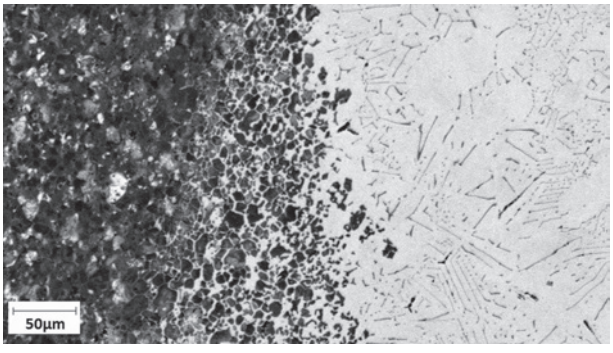

Fig. 8: SEM-BSE image of the penetration zone in experiment 6 (Fe-TiCMo B)

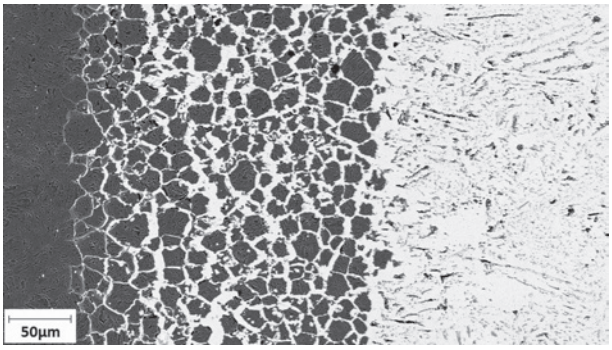

Fig. 9: SEM-BSE image of the penetration zone in experiment 8 (FeMo3.5-TiC B)

clearly much denser than after the experiments especially in the penetration zone compared to Figures 8 and 9. In all the experiments the melt penetrated into the substrate along the grain boundaries as depicted in Figures 8 and 9. The lighter phases in Figure 7 represent the Mo rich phases and the Mo content of the substrate was analysed to be 14.25 mass% (square in Fig. 7).

From Figures 8 and 9 the difference between the TiC and TiCMo can be clearly observed. In experiment 8 the penetration is much stronger and the grain size of the substrate bigger than in experiment 6 although the initial grain size of the powder used for making the TiCMo substrate was bigger. The melt seems to dissolve the TiCMo particles more strongly but it does not penetrate that strongly into the substrate. The lighter phases in TiCMo are the Mo-rich phases. In experiment 10 (304-TiCMo B) the penetration zone was very similar to Fig. 8.

3.3 Results of SEM-EDS analyses

Table 3 represents the average analyses of TiC/TiCMo substrate (dark grey and grey in Fig. 10 and Fig. 11) and the alloy phase (white in Fig. 10 and Fig. 11) surrounding the substrate particles in the penetration zone in experiments 1–3 and 5–8 (experiments with 304 excluded).

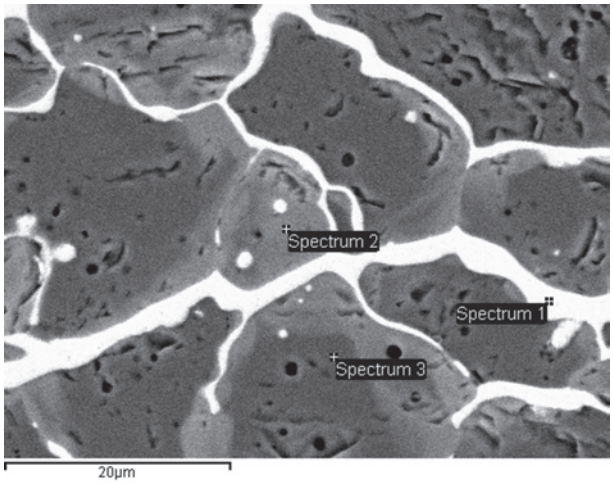

Fig. 10: SEM-BSE image of penetration zone in experiment 2 (FeMo5.2-TiC A) [22]

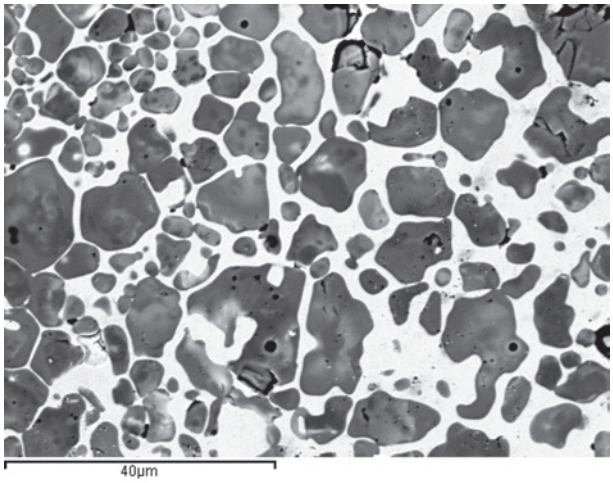

Fig. 11: SEM-BSE image of the penetration zone in experiment 6 (Fe-TiCMo B)

From Table 3 and from Fig. 10 it can be observed that in experiments 2 (FeMo5.2-TiC A) and 3 (FeMo3.7-TiC A), where the FeMo alloy was used, light grey rim phase formed on the surface of almost all of the TiC substrate

Table 3: Average analysis of TiC substrate and the alloy phase in the penetration zone (in mass%)

Experiment		Substrate core/dark			Substrate rim/light			Alloy phase	
		Ti	Fe	Mo	Ti	Fe	Mo	Ti	Mo
1	Fe-TiC A	81.5–83.2	0–2.2	–	–	–	–	2.6–3.0	–
2	FeMo5.2-TiC A	82.7–83.1	0–0.8	0	65.7–67.0	0–1.5	10.9–13.6	2.9	0
3	FeMo3.7-TiC A	80.7–81.4	0.6–1.1	0	68.1	1.1	9.1	0.7–1.6	0
5	Fe-TiC B	72.2–78.0	0–1.3	–	–	–	–	1.9–2.7	–
6	Fe-TiCMo B	63.1–81.7	0–2.7	0–12.1	43.3–50.6	0–2.1	24.3–31.4	1.1–2.1	0
7	Fe-TiCMo B 3	67.2–74.4	0.7	4.7–11.9	49.1	1.1	28.8	0.8–2.0	0
8	FeMo3.5-TiC B	71.9–81.4	0.3–2.3	0	61.2	4.4	8.8	1.1–2.4	0

particles in the penetration zone. This is the typical core rim-structure found in Ti and Mo containing carbides. No TiC particles with Mo present in the whole particle were found. There was always a Mo free core. The Mo content in the rim phase was higher in experiment 2 than in experiment 3. In experiment 8 (FeMo3.5-TiC B) the rim phase was observed only at very few TiC substrate particles. This is due to the longer holding period and the reactions during heating in type A experiments 2 and 3 and due to the faster cooling of the samples in type B experiment 8. In experiment 8 there was no time for the Mo to react with TiC to form the rim structure. The alloy phase surrounding the TiC substrate does not contain any Mo either. This is the case in all experiments with Mo present in the system (experiments 2–3 and 6–8), resulting from all Mo reacting with either the existing TiC particles or with dissolved Ti and C.

In experiments with the TiCMo substrate the Mo contents are very scattered as a result of the Mo being present in substrate. In the penetration zone it is present in almost all the substrate particles. However due to the Mo being present already in the substrate prepared by the SHS method no core-rim structure has been observed in the penetration zone (Fig. 11). Instead the Mo rich parts appear lighter and the lighter phases are randomly distributed in the TiCMo substrate particles.

Table 4 represents the average analyses of big TiC particles and the alloy phase on the droplet side in experiments 1–3 and 5–8 (experiments with 304 excluded). Small and/or thin TiC particles on the droplet side could not be analysed precisely due to the effect of the matrix (alloy phase).

On the droplet side in experiments 2 and 3 Mo was observed in the rim phase and also in (Ti,Mo)C particles where Mo was found in the whole particle (Fig. 12). The Mo content in the particles is slightly higher in experiment 2 with the higher initial Mo content in the alloy. Mo was not found in the core of the core-rim type particles. In experiment 8 (FeMo3.5-TiC B) Mo was observed only in the whole

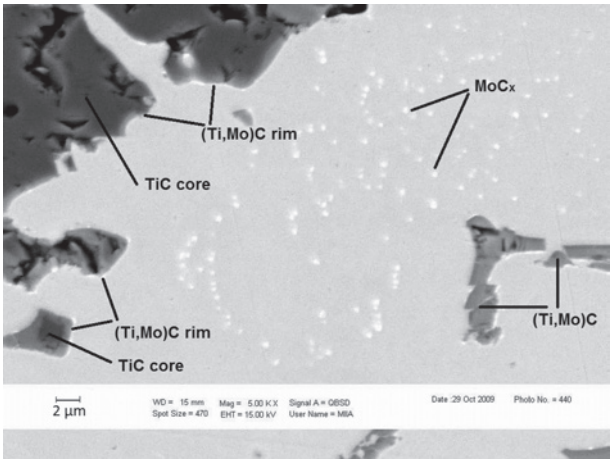

Fig. 12: SEM-BSE image of TiC and (Ti,Mo)C particles in experiment 2 (FeMo5.2-TiC A) [22]

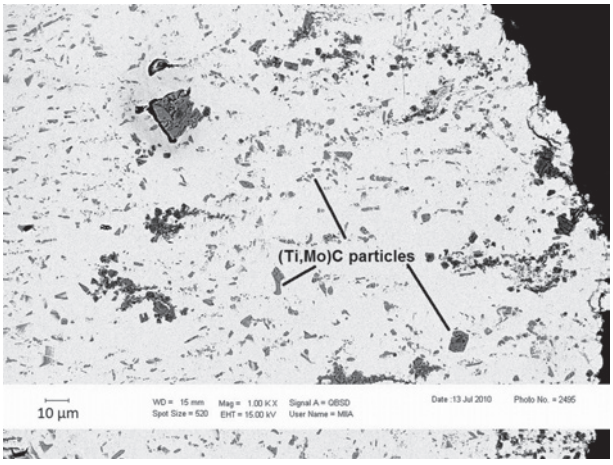

Fig. 13: SEM-BSE image of TiC and (Ti,Mo)C particles in experiment 8 (FeMo3.5-TiC B)

TiC particle and not as a rim phase on the TiC particles (Fig. 13). These Mo containing TiC particles were lighter in color, more homogenous and no lighter rim phase existed on the surface.

Table 4: Average analysis of TiC particles and the alloy phase (droplet material) on the droplet side (in mass%)

Experiment		TiC core/dark			TiC rim/light			Droplet phase	
		Ti	Fe	Mo	Ti	Fe	Mo	Ti	Mo
1	Fe-TiC A	78.4–85.1	1.2–5.4	–	–	–	–	0–0.6	–
2	FeMo5.2-TiC A	82.1–83.2	0–2.7	0	50.9–54.5	1.9–7.2	21.1–24.7	0–1.9	0
3	FeMo3.7-TiC A	75.9–81.5	1.1–8.2	0	52.3–67.5	1.6–4.1	7.8–21.3	0–0.4	0
5	Fe-TiC B	72.6–76.6	0.9–2.1	–	–	–	–	0–1.7	–
6	Fe-TiCMo B	63.0–71.0	0.8–1.6	0–12.0	63.9–69.7	2.8–3.5	7.5–11.5	0–0.7	0–0.6
7	Fe-TiCMo B3	69.0–78.1	1.4–7.5	4.6–9.6	62.5–65.2	2.1–3.0	10.7–12.6	0	0
8	FeMo3.5-TiC B	74.6–81.6	1.8–5.6	0	56.0–65.3	1.3–2.7	8.2–20.4	0–2.7	0

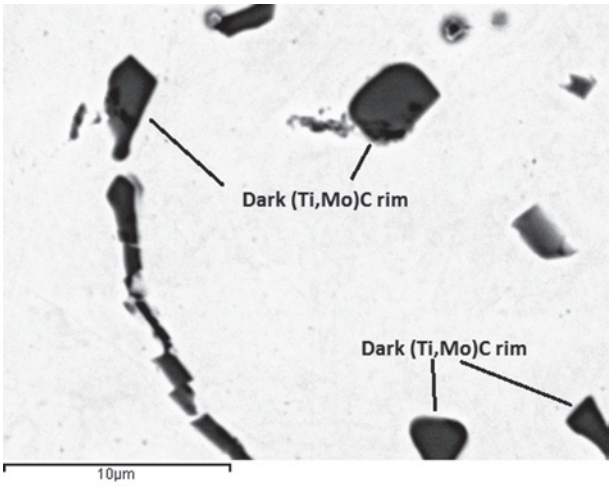

Fig. 14: SEM-BSE image of (Ti,Mo)C particles with a darker outer rim phase in experiment 10 (Fe-TiCMo B 3)

In addition some especially small particles (<5 µm) with a clearly darker rim phase were observed in all FeMo experiments (Fig. 14) both small spherical as well as thin and longish. They always contained Mo in the whole particle but the outer darker rim could not be precisely analyzed due to its small size. However the darker rim suggests a lower Mo content in the rim than in the core. Overall many TiC particles (big, small spherical and thin longish) on the droplet side in FeMo experiments 2, 3 and 8 contained Mo either in the rim phase or as a whole (Ti,Mo)C particle. The alloy did not contain any Mo and the Ti contents were clearly lower than in the alloy in the penetration zone (Table 3). Also very small white particles were observed in the alloy in experiments 2 and 3 (Figure 12). These phases were probably a MoC_x with a very small dissolved Ti content.

In the experiments with TiCMo substrate (6 and 7) the Mo containing particles found on the droplet side are usually quite evenly colored and they do not contain such clearly different phases as the substrate particles. Only a few substrate-like particles with randomly distributed lighter Mo rich phases were found. Core-rim structures with lighter surface were not observed. But as well as in the FeMo experiments also in the TiCMo experiments especially small (Ti,Mo)C particles with a darker rim phase were observed. The Mo contents of all types of particles are not that high (usually <12 mass%) but almost all particles contain Mo. Ti content in the alloy on the droplet side is very low or zero and Mo is basically zero. Low Mo content was measured at one point in experiment 6. It has to be pointed out that some of (Ti,Mo)C particles on the droplet side are so small that they cannot be precisely analyzed. In other words the existence of core-rim structure in the very small TiC particles (<2 µm) cannot be fully excluded. At least in bigger particles it was not observed. In general experiments 6 and 7 were very similar even though the holding period was different. Compared to FeMo experiments (2, 3 and 8) the TiC particles have lower Mo contents but the number of Mo containing TiC particles on the droplet side is clearly higher. The Mo contents in the particles in TiCMo experiments (6 and 7) are very similar and in the FeMo experiments (2, 3 and 8) more diverse.

The results from SEM-EDS analyses for experiments with stainless steel 304 (4, 9 and 10) are presented in Tables 5 and 6. In experiment 4 (304-TiC A) the substrate particles in the penetration zone have not reacted with the stainless steel at all and in experiments 9 (304-TiC B) and 10 (304-TiCMo B) the Fe and Cr contents in the TiC and TiCMo substrate are low. The Mo content in the substrate in penetration zone in experiment 10 changes very much

Table 5: Average analysis of TiC particles and the alloy phase in the penetration zone of experiments with stainless steel 304 (in mass%)

Experiment		Substrate					Alloy phase		
		Ti	Fe	Cr	Ni	Mo	Ti	Cr	Ni
4	304-TiC A	80.0–80.9	0	0	0	0	1.3–1.4	19.8–20.8	8.2–8.7
9	304-TiC B	80.1–81.9	0–1.0	0–1.7	0	0	0.8–2.2	13.5–18.1	8.9–9.6
10	304-TiCMo B	38.1–76.1	0–1.4	0–1.4	0	0–36.3	0.8–2.2	17.1–19.1	7.6–8.8

Table 6: Average analysis of TiC particles and the alloy on the droplet side of experiments with stainless steel 304 (in mass%)

Experiment		TiC					Droplet phase		
		Ti	Fe	Cr	Ni	Mo	Ti	Cr	Ni
4	304-TiC A	69.1–83.8	1.0–1.9	0.7–2.4	0	0–4.4	0–0.6	19.2–24.8	8.2–9.5
9	304-TiC B	69.0–79.4	0.9–2.8	1.0–3.9	0	0–7.8	0–0.5	16.6–20.6	8.4–9.2
10	304-TiCMo B	54.3–73.3	0.9–4.5	1.3–3.4	0	4.6–12.6	0–0.4	17.0–25.5	8.3–10.2

depending on where the analyses were taken like also in experiments 6 and 7 (Table 3). No Mo was found in the penetration zone in experiments 4 and 9.

On the droplet side in experiments 4 and 9 (TiC substrate) Mo was observed in a few longish/thin and small TiC particles only but not as rim phase. The reason for the small amount of Mo containing TiC particles and the low Mo content in them is the low Mo content of the 304. Experiment 10 is very similar to experiments 6 and 7 with TiCMo substrates used also. The small spherical and thin longish eutectic particles in the droplet alloy always contained some Fe and Cr. No light rim particles but some especially small particles with a darker rim were observed and all particles on the droplet side seem to contain Mo but not in very high contents (<13 mass%). Cr and Fe contents of the TiC particles are higher on the droplet side. Ni was not found in any of the (Ti,Mo)C or TiC particles in the experiments with stainless steel as well as previous experiments with FeNi alloy [2].

Overall three different shapes of TiC/(Ti,Mo)C particles can be found on the droplet side (Figure 15): 1) small spherical, 2) thin and longish eutectic carbides and 3) big angular or roundish particles [2].

In experiments 2 and 3 the occurrence of all these three particles was very strong. In experiment 4 all three types were observed but big particles not as strongly as in experiments 2 and 3. The reasons for the quite similar occurrence of all three particle types is due to the reactions during heating, the longer holding period and smaller cooling rate as well as observed in earlier experiments [2]. In the FeMo experiments 2 and 3 the interaction between the substrate and alloy seems to have been strongest, because of the occurrence of high amounts of big substrate-like particles on the droplet side. In type B experiments 6–10 all particle types were also found but not in similar amounts. The droplet side in experiments 6–10 contained a lot of small spherical and thin longish TiC/(Ti,Mo)C particles but only a few big particles. Also the density of particles overall was lower in type B experiments than in type A experiments. All this was due to no reactions during heating, shorter holding period and higher cooling rate in type B experiments. The main differences between the type A and type B are the strong dissolution and transportation of substrate particles onto the droplet side in and an overall higher density of TiC particles in type A experiments. Any big differences in the particle density and types were not observed between different type B experiments. In the 304 experiments (4, 9 and 10) CrC_x and sigma phase were also found. The Cr carbides were discussed in more detail in the previous article by the author [2].

A summary of the different types of carbide particles found in all experiments is presented in Table 7. From Table 7 it can be observed quickly that (Ti,Mo)C particles are found in all experiments containing Mo. Particles with a light, Mo-rich rim are found mainly in FeMo type A experiments (2 and 3), in which the FeMo alloy has time to react with the TiC particles to form the rim. Some (Ti,Mo)C particles with a dark, Mo-depleted rim were also found in almost all Mo containing experiments. In 304-TiC experiments (4 and 9) dark rim particles were not found because of the very low Mo content. In experiments with FeMo alloy the carbides contained more Mo than in the experiments with the TiCMo substrate. But in experiments with TiCMo substrate the number of carbides containing Mo was higher. In 304 experiments Cr was found in many carbides as well.

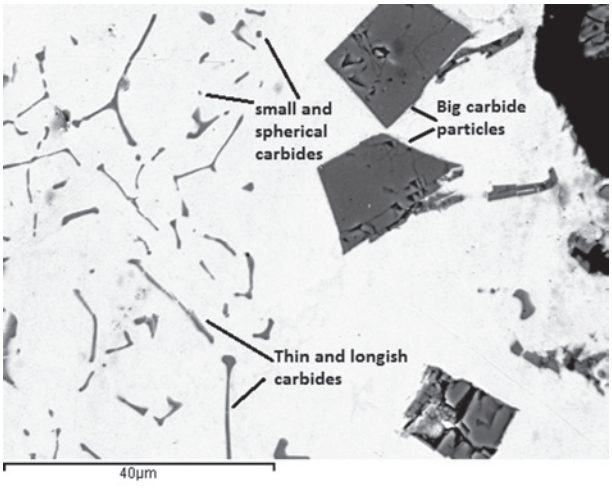

Fig. 15: SEM-BSE image of the alloy droplet in experiment 6 (Fe-TiCMo B)

3.4 Discussion

By comparing the results from this article and the previous article [2] it can be observed that the lowest contact angles were received by alloying the Fe with Ni or Mo. This was, however, the case in only type A experiments. In type B experiments the lowest contact angles were received by using TiCMo substrate although it was only a minor effect. It has to be kept in mind that TiCMo substrate was not used in type A experiments. It was only chosen for type B experiments which resembled the actual casting experiments [1]. A higher Mo content in the Fe-alloy might improve the wettability more strongly. The experiments with FeNi had the strongest penetration followed by FeMo and FeCr [2] resulting in strong interaction between the

Table 7: Summary of the different carbides found in the experiments

Experiment					Carbides					Other
No.	Material	Type	Holding period		Penetration zone		Droplet side			
			T (K)	t (min)	Light rim	TiC/(Ti,Mo)C	Light rim	Dark rim	TiC/(Ti,Mo)C	
1	Fe-TiC	A	1823	30	No	All TiC	No	No	All TiC	–
2	FeMo5.2-TiC	A	1823	15	All	No	Some	Some small	Some (Ti,Mo)C	Many carbides contained Mo, Mo contents higher than in TiCMo experiments
3	FeMo3.7-TiC	A	1823	15	All	No	Some	Some small	Some (Ti,Mo)C	Many carbides contained Mo, Mo contents higher than in TiCMo experiments
4	304-TiC	A	1748	15	No	All TiC	No	No	Few (Ti,Mo)C	Many carbides contained small amounts of Cr
5	Fe-TiC	B	1823	10	No	All TiC	No	No	All TiC	–
6	Fe-TiCMo	B	1823	10	No	All (Ti,Mo)C	No	Some small	Many (Ti,Mo)C	All carbides contain Mo but lower than in FeMo experiments
7	Fe-TiCMo	B	1823	3	No	All (Ti,Mo)C	No	Some small	Many (Ti,Mo)C	All carbides contain Mo but lower than in FeMo experiments
8	FeMo3.5-TiC	B	1823	10	Some	Many (Ti,Mo)C	No	Some small	Many (Ti,Mo)C	Many carbides contained Mo, Mo contents higher than in TiCMo experiments
9	304-TiC	B	1823	10	No	All TiC	No	No	Few (Ti,Mo)C	Many carbides contained small amounts of Cr
10	304-TiCMo	B	1823	10	No	All (Ti,Mo)C	No	Some small	Many (Ti,Mo)C	All carbides contained some Mo, small amounts of Cr in many carbides as well

substrate and the alloy. The experiments with stainless steel as the droplet material did not seem to have a significant effect on the wetting compared to pure Fe. The Ni content in the 304 was similar to the Ni content used in the Fe-alloy experiments [2] but the Mo content was very low. It seems that Cr and Ni overrule the effects of each other on the wettability. The penetration in the stainless steel 304 was very strong especially in type A experiment due to the combined effect of Ni and Cr. As a comparison the contact angle in TiC-NiMo based cermets with 10 mass% Mo in the binder Ni was measured by Hussainova et al. [14] to be 0° which means complete wetting. Complete wetting was not observed in any of the experiments done in this study. Regarding the casting of TiC/TiCMo reinforced stainless steel [1] both the initial and the minimum contact angle are important. Good wetting i.e. low contact angle results in good bonding between the reinforcement and the matrix material and in a desired distribution of the particles. In most experiments already the initial contact angles were low. In some experiments (2, 3 and 8) the initial contact angles were somewhat higher (around 90 °C), but the contact angle was decreased very quickly to very low values meaning good wettability between the substrate and the metal/alloy. Only exception was experiment 4 (304-TiC A) with a clearly lower holding temperature.

The TiC/TiCMo and Fe/FeMo/stainless steel systems can contain different kinds of carbide particles: plain TiC particles, TiC particles with a lighter (Ti,Mo)C rim, plain (Ti,Mo)C particles, (Ti,Mo)C particles with a Mo depleted darker rim and also CrC_x rich particles. These particle types can exist in different shapes as well. The different types of TiC and (Ti,Mo)C particles found in the systems contain very different amounts of Ti and Mo. During the holding period and probably also during heating in type A experiments the substrate (TiC or TiCMo) strongly dissolved into the alloy and TiC particles started to appear on the droplet side due to drifting from the substrate as well as precipitation of dissolved Ti, C and Mo. This resulted in carbides with different chemistries. The dissolution and precipitation of carbides have been discussed in detail in the previous article by the author [2]. Experiments 6 and 7 with pure Fe and TiCMo substrate but with different holding times were performed in order to observe the dissolution of the substrate. These experiments did not differ that much from each other. The penetration of the liquid was clearly stronger in experiment 6 with the longer holding but the TiC particles and the amounts formed are

very similar. This means that the dissolution of TiCMo substrate is very fast and the saturation is reached quite quickly resulting in quite strong (Ti,Mo)C formation on the droplet side. The same phenomenon was observed in the Fe-TiC experiments [2]. The equilibrium condition of the dissolution and precipitation is probably reached already in 3 minutes. The good wettability between the different systems is ensuring the high reactivity at the interface. In all experiments especially the amount of small spherical and thin longish TiC and (Ti,Mo)C particles was high (Fig. 12, 13 and 15). These carbides have precipitated from the melt due to the high dissolution of the substrate. The (Ti,Mo)C particles observed were probably formed during solidification partly directly from the eutectic melt and partly by Mo in the melt reacting with existing TiC, which were already formed during the holding period. The existence of small spherical and thin longish TiC was somewhat stronger in type A experiments due to the differences in the experimental procedures. In this study the low Ti and Mo contents of the alloy droplet probably resulted from the strong precipitation of carbides. Mo content of the alloy was basically zero in all experiments.

Molybdenum and titanium contents of the (Ti,Mo)C particles, the rim phases of TiC particles as well as the substrate particles are presented in Figure 16.

In the TiCMo substrate the TiC is partly replaced by MoC_x. This seems to be the case also in other Mo containing TiC particles found in the alloy droplet in all experiments. The carbon content remains high in all Mo containing particles and it can be concluded that TiC is partly replaced by MoC_x. Cedat et al. [24] have studied the microstructure of Mo composites with TiC and found out that the (Ti,Mo)C observed in the samples appears with a composition close to the solid-solubility of TiC-$Mo_{10–15at\%}$. They found (Ti,Mo)C phase all around each TiC particle. In the experiments of this paper the Mo content was mainly below 12 at%. The Mo contents of the particles vary with the initial Mo which has been observed also by Cutard et al. [13]. Experiments with 304 stainless steel and TiC have not been included in Fig. 16 but they contained clearly less Mo. However it has to be pointed out that the small and longish particles are not included in Fig. 16 because they could not be analyzed accurately due to the strong effect of the surrounding alloy.

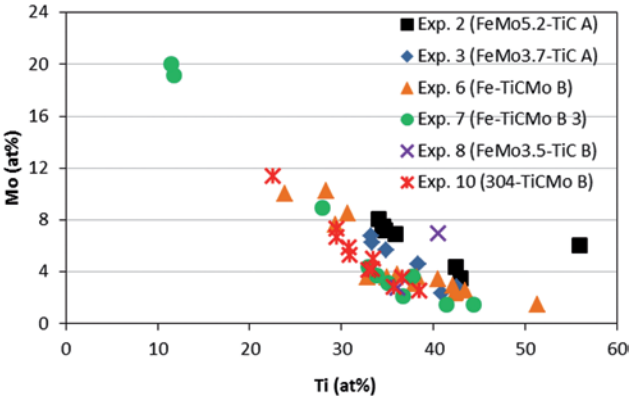

Fig. 16: Molybdenum and Titanium contents in TiC particles containing Mo

In the experiments of this study three types of Mo containing particles have been observed: TiC particles with a lighter Mo containing rim phase, (Ti,Mo)C particles with darker rim phase and plain (Ti,Mo)C. The TiC particles with a lighter rim phase (Fig. 12) were clearly observed only in experiments 2, 3 and 8 with the FeMo alloy and TiC substrate. They were usually big carbides (>10 μm) but a few small ones have been found in the alloy droplet. Several mechanisms have been proposed for the formation of these TiC and Ti(C,N) particles with a Mo containing rim around the particles [16, 25]. Based on the experiments of this study FeMo melt reacts with the existing TiC substrate particles in the penetration zone, interface and alloy droplet resulting in (Ti,Mo)C, which is in accordance with Qian et al. and Andrén et al. [16, 25]. In the experiments 2 and 3 these particles are found everywhere but in experiment 8 (type B) only a few in the penetration zone and at the interface. The melt infiltrated quite strongly into the substrate but it did not have enough time to react with the substrate to form (Ti,Mo)C on the surface. In experiment 8 there were no reactions between the substrate and the alloy during heating, the holding period was shorter and the cooling down to 1673 K faster. The particles with a lighter rim were probably formed partly during heating and during solidification, because their formation in experiment 8 was very small. In type B experiments the penetration of the melt into the substrate was strong but due to the above-mentioned differences in the experiments of types A and B only a few substrate particles had drifted to the droplet side. In type A experiments the drifting was stronger and more TiC particles appeared on the droplet side. Mo, Ti and C dissolved in the melt could precipitate on these particles and form a lighter rim phase. None of the big substrate-like particles in type B experiments had a lighter rim phase, but in type A many of the big TiC particles had. These lighter rim particles have not been found in the experiments with TiCMo substrate (6, 7 and 10) because no plain TiC particles existed. Instead only more homogenous (Ti,Mo)C particles and some TiC particles with randomly distributed lighter Mo rich phases in the particles are found. These particles with the

random light phases are most probably originating from the substrate.

The carbides with a darker rim phase (Fig. 14) have been found in all Mo containing experiments also. Their occurrence is not nearly as strong as of the more homogenous (Ti,Mo)C particles. The particles are usually small spherical or thin longish eutectic carbides and they always contain Mo in the whole particle. The dark rim is very thin and cannot be precisely analyzed, but it is evident that the rim is depleted in Mo. These darker rim particles have been observed in other studies as well [26–27]. According to Chen et al. [26] in solid-liquid reaction couple of $(Ti_{0.9}Mo_{0.1})C$-Ni these particles are formed by precipitation of Mo depleted (Ti,Mo)C particles on undissolved larger carbides leading to more dissolution of (Ti,Mo)C particles and re-precipitation of Mo depleted carbides. If the original carbide is completely surrounded by the Mo depleted carbide the original carbide will be sealed off from the liquid and a bright core particle with a dark rim will form. The Mo depleted carbide might start precipitating also on only one favorable nucleation site on original carbide resulting in complete disappearance of the original particle which is one possible mechanism for the formation of homogenous (Ti,Mo)C particles. During cooling the Mo-rich melt might form Mo-rich carbide on this dark core resulting in a bright rim/dark core particle [26]. That phenomenon was not, however, observed in this study due to quite fast cooling rate.

In the actual casting experiments in the context of this study [1] a TiCMo insert and stainless steel were used. Experiment 10 (304-TiCMo B) simulated best the actual casting process. In the castings [1] most of the carbide particles had a lighter rim phase with higher Mo content and they were small and spherical. In experiment 10 of this study these particles were not observed. The differences affecting the phenomena were evidently the higher temperature in castings, smaller TiCMo/stainless steel ratio and the very slow cooling of the castings. In both type A and B experiments a lot of small and thin (Ti,Mo)C particles with no lighter rim phase were found, but these particles were not reported in the castings [1]. The longer the time for the carbides and the alloy or steel to react and the slower the cooling, the more rim-core particles existed. Consequently, it can be stated that most of the core-rim structures are formed during solidification. In the wetting experiments there is not so much time for them to form especially in type B experiments.

The formation of different carbides in 1273–1873 K was calculated by Factsage 6.3 [28] using FSstel database (Fig. 17). The composition was chosen based on the 304 stainless steel with 10 and 2.2 mass% TiCMo. The composition

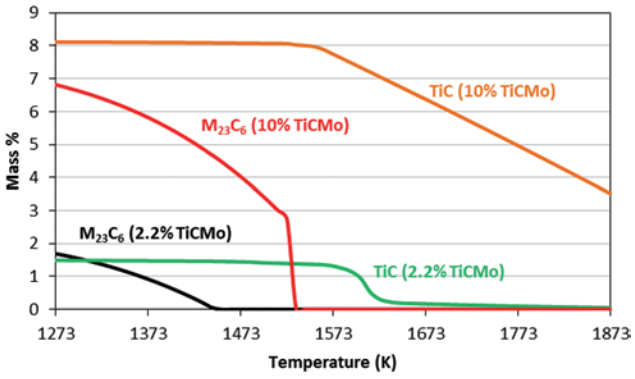

Fig. 17: Formation of different carbides at 1273–1873 K in Fe-Ti-C-Cr-Ni-Mo-Mn-Si-O-N-S systems

of the 304 in the calculation with 10 mass% TiCMo was 20 mass% Cr, 9 mass% Ni, 0.3 mass% Mo, 0.02 mass% C, 1.0 mass% Mn, 0.5 mass% Si, 100 ppm O, 200 ppm N, 300 ppm S and balance Fe. In the calculation with 2.2 mass% TiCMo the composition was otherwise the same except for Cr and Ni, 21.7 mass% and 9.7 mass% respectively.

Besides TiC a $M_{23}C_6$ type carbide is formed in both calculations. According to the calculations the main constituent of this carbide is $Cr_{20}Mo_3C_6$ and two other main constituents are $Cr_{23}C_6$ and $Fe_{20}Mo_3C_6$. M_2C type carbide like Mo_2C was not formed at this temperature. Most probably Mo is present in the TiC in addition to the other carbides. However, these calculations are not able to show Mo, Fe or Cr in the solid TiC. According to the calculation with 10 mass% TiCMo addition the TiC formation is stronger than the $M_{23}C_6$ formation. In the calculation with 2.2 mass% TiCMo added the formation of $M_{23}C_6$ is stronger but the formation starts at lower temperatures. Overall the formation of $M_{23}C_6$ starts at clearly lower temperatures (<1550 K) than the formation of TiC which is already present in the melt. In experiments 4, 9 and 10 carbides rich in Cr with some Fe and very small Ti content were clearly observed in the droplet. In experiment 10 with TiCMo substrate some of these carbides contained Mo (<6 mass%) and some contained small amounts of Ti (<1 mass%).

Results can be compared with Bourithis et al. [29] who studied laser surface alloying of low alloyed steel by TiC, Mo, Cr and C containing powder and found two types of carbides based on the chemical composition: a carbide containing >80 mass% Ti and a MC type carbide with Ti and some Mo, Cr and Fe. They proposed that the MC type lighter rim carbides are formed due to the melt becoming poorer with Ti after precipitation of TiC. They reported the eutectic carbides and the globular carbides as MC type, which is the case in this study also. All small, spherical and eutectic carbides in experiments with 304 stainless

steel contained Fe and Cr and in experiment 10 also Mo. It seems that in TiC or TiCMo and stainless steel systems several different carbides with very complex shapes and chemistries can form.

4 Conclusions

Wetting experiments using TiC or TiCMo as substrate and pure Fe, FeMo or stainless steel type 304 have been performed and analyzed for wetting, dissolution and carbide formation.

1. The wettability between liquid Fe and TiC somewhat improved when iron was alloyed with 3–5 mass% Mo in type A experiments. In type B experiments with shorter contact time any corresponding decrease in the contact angle was not observed due to Mo. A very small decrease in the contact angle was observed by using TiCMo substrate instead of TiC. The wetting between stainless steel and TiC or TiCMo substrate was not improved compared to pure Fe.
2. All dissolved Mo was stated to react with Ti and C to form (Ti,Mo)C on existing TiC particles or during solidification. Especially the occurrence of small homogenous (Ti,Mo)C with no rim-core structure was plentiful due to the strong dissolution of the substrate into the melt. Any Mo could not be detected in the alloy phase.
3. Rim-core types particles existed with both a brighter Mo rich rim and darker Mo depleted rim. Lighter rim particles were only observed when Mo was added with the alloy as $FeMo_x$. Darker rim particles were observed in all Mo containing experiments. A longer time at higher temperatures resulted in stronger formation of lighter rim particles.
4. Overall the carbides formed in TiC/TiCMo and Fe/FeMo/stainless steel systems were very complex. Carbides can exist with complex chemistries and shapes. This complex nature of the carbides has to be taken into account while developing the manufacturing processes of metal-matrix composites especially when high alloyed stainless steel is used.

Acknowledgments: The Research Group for Advanced and Functional Materials at Aalto University School of Chemical Technology is acknowledged for preparing the TiC substrates by Spark-Plasma-Sintering (SPS) Technique. M.Sc. (Tech.) Hannu Heikkinen is acknowledged for performing part of the experiments and the analyses which were presented in his master's thesis.

Funding: The Finnish Funding Agency for Technology and Innovation (TEKES) is acknowledged for funding this study.

Received: August 29, 2013. Accepted: January 18, 2014.

References

[1] J. Tiusanen, K. Rissa, T. Ritvonen, J. Lagerbom, K. Keskiaho and T. Lepisto, *Est. J. Eng.*, **15**, (4), 293–300 (2009).
[2] M. Kivio, L. Holappa, T. Yoshikawa and T. Tanaka, *High Temp. Mater. Proc.*, **31**, 645–656 (2012).
[3] V. Kuzucu, M. Aksoy and M. H. Korkut, *J. Mater. Process. Technol.*, **82**, 165–171 (1998).
[4] A. Pardo, M. C. Merino, A. E. Coy, F. Viejo, M. Carboneras and R. Arrabal, *Acta Mater.*, **55**, 2239–2251 (2007).
[5] J. H. Jang, C. H. Lee, Y. U. Heo and D. W. Suh, *Acta Mater.*, **60**, 208–217 (2012).
[6] G. V. Samsonov, G. T. Dzodziev, L. I. Klyachko and V. K. Vitryanyuk, *Powder Metall. Met. C+*, **11**, (4), 300–302 (1972).
[7] D. Vallauri, I. C. Atias Adrian and A. Crysanthou, *J. Eur. Ceram. Soc.*, **28**, 1697–1713 (2008).
[8] S. Zhang, *Mater. Sci. Eng., A*, **A163**, 141–148 (1993).
[9] D. S. Park, Y. D. Lee, T. Jung and S. Kang, *Korean J. Ceram.*, **5**, (3), 230–234 (1999).
[10] S. Q. Zhuo, W. Zhao, W. H. Xiong and Y. N. Zhou, *Acta Metall. Sin. (Engl. Lett.)*, **31**, (3), 211–219 (2008).
[11] H. O. Andrén, *Mater. Des.*, **22**, 491–498 (2001).
[12] S. Cardinal, A. Malchere, V. Garnier and G. Fantozzi, *Int. J. Refract. Met. Hard Mater.*, **27**, 521–527 (2009).
[13] T. Cutard, T. Viatte, G. Feusier and W. Benoit, *Mater. Sci. Eng., A*, **A209**, 218–227 (1996).
[14] I. Hussainova, *Wear*, **255**, 121–128 (2003).
[15] D. Mari, S. Bolognini, G. Feusier, T. Cutard, C. Verdon, T. Viatte and W. Benoit, *Int. J. Refract. Met. Hard Mater.*, **21**, 37–46 (2003).
[16] M. Qian and L. C. Lim, *J. Mater. Sci.*, **34**, 3677–3684 (1999).
[17] C. Y. Chen, H. W. Yen, F. H. Kao, W. C. Li, C. Y. Huang, J. R. Yang and S. H. Wang, *Mater. Sci. Eng., A*, **499**, 162–166 (2009).
[18] J. I. Erauskin, A. Sargyan and J. L. Arana, *ISIJ Int.*, **49**, 4, 582–586 (2009).
[19] Y. Funakawa, T. Shiozaki, K. Tomita, T. Yamamoto and E. Maeda, *ISIJ Int.*, **44**, (11), 1945–1951 (2004).
[20] A. T. Evtushenko, S. Pazare and S. S. Torbunov, *Met. Sci. Heat Treat.*, **49**, (3–4), 200–203 (2007).
[21] G. V. Samsonov, A. D. Panasyuk and G. K. Kozina, *Powder Metall. Met C+*, **7**, (11), 874–878 (1968).
[22] H. Heikkinen, *Wetting of titanium carbide and iron alloys*, Master's thesis (In Finnish), Helsinki University of Technology, p. 87, (2009).
[23] Z. Liu and H. Fredriksson, *Metall. Mater. Trans. A*, **28A**, 471–483 (1997).
[24] D. Cedat, M. Clavel, J. H. Schmitt, M. Le Flem and A. Allemand, *J. Nucl. Mater.*, **385**, 533–537 (2009).
[25] H. O. Andrén, U. Rolander and P. Lindahl, *Appl. Surf. Sci.*, **76–77**, 278–284 (1994).

[26] L. Chen, W. Lengauer, P. Ettmayer, K. Dreyer, H. W. Daub and D. Kassel, *Int. J. Refract. Met. Hard Mater.*, **18**, 307–322 (2000).
[27] N. Liu, S. Chao and X. Huang, *J. Eur. Ceram. Soc.*, **26**, 3861–3870 (2006).
[28] Factsage 6.3: http://www.factsage.com/
[29] L. Bourithis, A. Milonas and A. D. Papadimitriou, *Surf. Coat. Technol.*, **165**, 286–295 (2003).